

Cancellation of small- x divergences in the three-gluon-vertex Hamiltonian with canonical gluon mass

Juan José Gálvez-Viruet^{✉*}

Departamento de Física Teórica, Universidad Complutense de Madrid, 28040 Madrid, Spain

María Gómez-Rocha^{✉†}

Departamento de Física Atómica, Molecular y Nuclear and Instituto Carlos I de Física Teórica y Computacional, Universidad de Granada, 18071 Granada, Spain



(Received 28 July 2023; accepted 14 September 2023; published 1 November 2023)

The front form of Hamiltonian dynamics provides a framework within QCD in which interaction terms are invariant under seven of ten Poincaré transformations and the vacuum structure is simple. However, canonical expressions are divergent and must be regulated before attempting to define an eigenvalue problem. The renormalization-group procedure for effective particles (RGPEP) provides a systematic way of renormalizing Hamiltonians and obtaining counterterms. One of its achievements is the description of asymptotic freedom with a running coupling defined as the coefficient of the three-gluon-vertex operators in the renormalized Hamiltonian. Yet, the results we obtain need a deeper understanding, since the coefficient function shows a finite cutoff dependence, at least in the third-order terms of the perturbative expansion. In this work, we present an RGPEP computation of the three-gluon vertex with a different regularization scheme based on massive gluons. Our calculation shows that the three-gluon Hamiltonian interaction term has a finite limit as the gluon mass vanishes, but the finite function $h(x)$ that was obtained in previous calculations as a consequence of the finite dependence on the regularization is different. This result indicates a need for understanding how to eliminate finite regularization effects from Hamiltonians for effective quarks and gluons in QCD. Nevertheless, it is remarkable that all terms depending on the gluon mass cancel out in the limit of vanishing gluon mass in a nontrivial way, even when each term individually diverges in such a limit.

DOI: [10.1103/PhysRevD.108.096001](https://doi.org/10.1103/PhysRevD.108.096001)

I. INTRODUCTION

The fundamental description of hadronic phenomena in quantum chromodynamics (QCD) presents severe and long-standing problems. The mathematical complexity of the theory, the impossibility of applying perturbation theory in the infrared regime, and the unapproachable need to deal with an infinite number of degrees of freedom have led many researchers to focus on phenomena that take place in a narrow energy range, adopting approximations and constructing effective theories or models valid for specific regimes. Indeed, it is not trivial how to reproduce QCD features of hadrons that occur at different energy scales within the same approach. While at low energy quantum

numbers of hadrons seem to be well explained by a small number of constituents, at high energies asymptotic freedom [1–4] of many weakly interacting particles dominates [5].

The renormalization-group procedure for effective particles (RGPEP) was developed to solve bound states in QCD. The method stems from the similarity renormalization group, formulated by Glazek and Wilson [6,7]. It is formulated in the front form of Hamiltonian dynamics [8] and introduces the notion of effective particles in quantum field theory [9].

The RGPEP provides a means for constructing a family of equivalent effective Hamiltonians depending on a scale parameter, which allows connecting different energy scales, and selecting the range of interest without truncating significant matrix elements. It introduces the concept of effective particles [9], which are related to canonical or pointlike ones by means of a unitary transformation.

The method has been applied to several theories [10–15], some of them simple enough to be solved exactly [16,17]. In the case of QCD, only perturbative solutions in powers of the coupling constant have been considered so far in the

*juagalve@ucm.es

†mgomezrocha@ugr.es

Published by the American Physical Society under the terms of the Creative Commons Attribution 4.0 International license. Further distribution of this work must maintain attribution to the author(s) and the published article's title, journal citation, and DOI. Funded by SCOAP³.

renormalization-group equation. For instance, the eigenvalue problems for heavy quarkonium and heavy baryons have been derived starting from QCD with only heavy quarks using the second-order Hamiltonian solution to the RGPEP equation. The quark-(anti)quark effective potential for effective quarks and gluons has been obtained, and the spectra of hadrons have been computed with unexpected accuracy [9,15].

Third-order calculations allowed us to analyze the structure of the three-gluon vertex [18,19]. From the coefficient of such structure, the running of the coupling constant was defined as its variation with the renormalization-group scale λ . The method turned out to reproduce correctly the property of asymptotic freedom [18,19]. Moreover, it was shown that the running of the coupling had a similar or identical form to the variation with virtual momenta that is obtained using Feynman diagrams for off-shell Green's functions. However, in Refs. [18,19], three different regularizations were considered, and a certain finite dependence on the choice of the regulating function was encountered, which needs deeper understanding.

This article concerns the study of a new regularization method for the QCD Hamiltonian within the RGPEP. Namely, we introduce an infinitesimal gluon-mass parameter m_g to regulate singularities that appear for gluons carrying a small longitudinal momentum fraction x . In other words, we allow gluons to have a nonzero canonical mass. This regularization allows us to circumvent the vacuum problem which appears only in cases $p^+ = 0$, producing infinity eigenvalues for $m_g \rightarrow 0$, a feature which is welcome because no free, colored particles are found in nature.

In particular, we consider again the third-order three-gluon-vertex Hamiltonian in the SU(3) Yang-Mills theory and explore the effect of such a regularization in the asymptotic freedom result. On a similar basis to what was done in [19], the running coupling is identified as the coefficient in front of the effective three-gluon-vertex Hamiltonian operator, which is derived by solving the RGPEP equation perturbatively.

Previous works collect a detailed description of formulas appearing at every step taken in perturbative RGPEP calculations [19,20]. In this document, we summarize the main steps and focus our attention on the new element considered here: the new regularization and its consequence in the interaction terms and running coupling. We see clearly how the dependence on the gluon mass cancels once all contributions to the three-gluon vertex in the limit $m_g \rightarrow 0$ are added, even though separate contributions diverge.

The regularization treated here was initially introduced in other problems addressed within the RGPEP [11,12,21]. Given the success of such studies and aiming at future high-order solutions to the RGPEP equation in QCD, we apply it here to the most difficult physical problem considered so far using this approach.

Other methods also include a canonical gluon mass for different considerations. For example, a Faddeev-Popov Lagrangian in the Landau gauge with a tree-level mass term [22] can reproduce the pion decay constant [23] and lattice gluon and ghost correlation functions [24] by means of perturbative calculations extended to the infrared regime. This is different from other studies on dynamical gluon-mass generation which is broadly explored from different approaches [25–32], including RGPEP [14,15,33].

The article is organized as follows. Section II presents the main and general steps of the RGPEP and the regularization method employed in this particular work. Section III provides the derivation of the three-gluon vertex and the resulting running coupling. Section IV concludes the article. Appendixes A and B with extended formulas are available at the end of the document.

II. THE METHOD

A. Front form of dynamics

The RGPEP uses the front form of dynamics [8,34]. In this form, four vectors in Minkowski space-time are denoted by $x^\mu = (x^+, x^-, x^\perp)$, where $x^+ = x^0 + x^3$, $x^- = x^0 - x^3$, and $x^\perp = (x^1, x^2)$. We use the Brodsky-Lepage notation [34]; the inner product is defined as

$$a \cdot b = a^\mu b^\nu g_{\mu\nu} = \frac{1}{2} a^+ b^- + \frac{1}{2} a^- b^+ - a^\perp b^\perp, \quad (1)$$

where summation over repeated indices is assumed. The “ $-$ ” component of the four momentum p^μ is then

$$p^- = \frac{p^{\perp 2} + m^2}{p^+} \quad (2)$$

and represents the energy of the particle.

Our starting point is the front-form Hamiltonian of QCD without quarks. The Hamiltonian density can be derived from the \mathcal{T}^{+-} component of the energy-momentum tensor $\mathcal{T}^{\mu\nu}$ associated with the corresponding Lagrangian density. Integration of \mathcal{T}^{+-} over the hypersurface $x^+ = 0$ leads to the (classical) front-form Hamiltonian

$$P^- = \frac{1}{2} \int_{x^+=0} dx^- d^2 x^\perp \mathcal{H}. \quad (3)$$

Canonical quantization requires replacing the field A^μ by the quantum operator \hat{A}^μ , defined by its Fourier expansion on the surface $x^+ = 0$:

$$\hat{A}^\mu = \sum_{\sigma c} \int [k] [t^c \varepsilon_{k\sigma}^\mu \hat{a}_{k\sigma c} e^{-ikx} + t^c \varepsilon_{k\sigma}^{\mu*} \hat{a}_{k\sigma c}^\dagger e^{ikx}]_{x^+=0}, \quad (4)$$

where $[k] = dk^+ d^2 k^\perp / (16\pi^3 k^+)$. For simplicity, we omit hats in operators in what follows. Creation and annihilation

operators $a_{k\sigma c}^\dagger$ and $a_{k\sigma c}$, satisfy the canonical commutation relation

$$[a_{k\sigma c}, a_{k'\sigma'c'}^\dagger] = k^+ \tilde{\delta}(k - k') \delta^{\sigma\sigma'} \delta^{cc'}, \quad (5)$$

where σ and c are spin and color indices, respectively. The momentum delta function is given by $\tilde{\delta}(p) = 16\pi^3 \delta(p^+) \delta(p^1) \delta(p^2)$, and the polarization four vectors have the components

$$\varepsilon_{k\sigma}^\mu = (\varepsilon_{k\sigma}^+ = 0, \varepsilon_{k\sigma}^- = 2k^\perp \varepsilon_\sigma^\perp / k^+, \varepsilon_\sigma^\perp). \quad (6)$$

The quantum canonical Hamiltonian is obtained after normal ordering of operators, represented by

$$\hat{P}^- = \frac{1}{2} \int dx^- d^2x^\perp : \mathcal{H}(\hat{A}) :. \quad (7)$$

Details of \hat{P}^- can be found in [18,19,35].

For pure gluonic QCD, only products of fields A^μ and of its derivatives are involved:

$$\mathcal{H} = \mathcal{H}_{A^2} + \mathcal{H}_{A^3} + \mathcal{H}_{A^4} + \mathcal{H}_{[\partial A A]^2}, \quad (8)$$

where \mathcal{H}_{A^2} is the free Hamiltonian, \mathcal{H}_{A^3} is the three-gluon vertex, \mathcal{H}_{A^4} is the four-gluon vertex, and $\mathcal{H}_{[\partial A A]^2}$ appears due to the constraint imposed on A^- by the Lagrange equations in the light-cone gauge $A^+ = 0$ (cf. Refs. [18,19,34] for details):

$$A^- = 2 \frac{1}{\partial^+} \partial^\perp A^\perp - g \frac{2i}{\partial^{+2}} [\partial^+ A^\perp, A^\perp]. \quad (9)$$

We will use the following notation. Hamiltonian terms with one creation and one annihilation operators are written using subscripts H_{11} . Likewise, terms with two creation and one annihilation operators are denoted by H_{21} . More generally, H_{ij} denotes a term with i creation and j annihilation operators.

The kinetic energy of *free* particles is independent of the coupling constant g :

$$\begin{aligned} H_{11} &= \frac{1}{2} \int_{x^+=0} dx^- d^2x^\perp : \mathcal{H}_{A^2} : \\ &= \sum_1 \int [1] \frac{k_1^{\perp 2} + m_g^2}{k_1^+} a_1^\dagger a_1, \end{aligned} \quad (10)$$

where we have used the abbreviation $[1] = [k_1]$. The subscript 1 in particle operators stands for spin s_1 , color c_1 , and momentum k_1 of particle 1. The parameter m_g is the canonical gluon mass, added to the QCD Hamiltonian. An extended discussion about this parameter will be given in the next section, where the regularization method is explained.

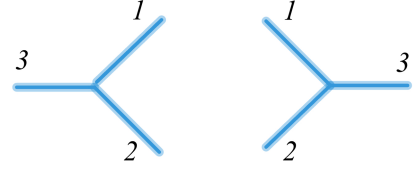


FIG. 1. First-order three-gluon vertex diagram. Left: term with two annihilation and one creation operators, $Y_{123}^* a_3^\dagger a_2 a_1$. Right: term with one annihilation and two creation operators, $Y_{123} a_1^\dagger a_2^\dagger a_3$.

The three-gluon vertex is proportional to g and has the form

$$\begin{aligned} H_{21} + H_{12} &= \frac{1}{2} \int_{x^+=0} dx^- d^2x^\perp : \mathcal{H}_{A^3} : \\ &= g \sum_{123} \int [123] f_{t_r} \tilde{\delta}(k^\dagger - k) Y_{123} a_1^\dagger a_2^\dagger a_3 + \text{H.c.}, \end{aligned} \quad (11)$$

where numbers 1, 2, and 3 in the creation and annihilation operators represent all quantum numbers of particles 1, 2, and 3, respectively, and the shortcut notation $[123] = [1][2][3]$ is used. The argument of the Dirac delta function $(k^\dagger - k)$ denotes differences of momenta of created particles minus annihilated ones in an interaction, respectively. These terms are represented in Fig. 1.

The momentum carried together by all annihilated or all created particles in a single interaction is called *parent* momentum. Conservation of momentum allows us to write $k_1^+ = x_1 k_3^+$, $k_2^+ = x_2 k_3^+$, with $x_1 + x_2 = 1$; and $k_1^\perp = x_1 k_3^\perp + \kappa_{12}^\perp$, $k_2^\perp = x_2 k_3^\perp - \kappa_{12}^\perp$, so that $\kappa_{12}^\perp = x_2 k_1^\perp - x_1 k_2^\perp$. We use the subscript i/p to denote the momentum of the daughter particle i relative to the parent p . For example, in a vertex $a_1^\dagger a_2^\dagger a_3$, the parent momentum is k_3 and $k_3^{\perp,+} = k_1^{\perp,+} + k_2^{\perp,+}$. We write $k_1^\perp = x_{1/3} k_3^\perp + \kappa_{1/3}^\perp$, where $x_{1/3}$ denotes x_1/x_3 and $\kappa_{1/3}^\perp = \kappa_{12}^\perp$.

The factor Y_{123} is a polarization function:

$$\begin{aligned} Y_{123} &= i f^{c_1 c_2 c_3} \left[\varepsilon_1^* \varepsilon_2^* \cdot \varepsilon_3 \kappa - \varepsilon_1^* \varepsilon_3 \cdot \varepsilon_2^* \kappa \frac{1}{x_{2/3}} \right. \\ &\quad \left. - \varepsilon_2^* \varepsilon_3 \cdot \varepsilon_1^* \kappa \frac{1}{x_{1/3}} \right] \end{aligned} \quad (12)$$

with $\varepsilon \equiv \varepsilon^\perp$ and $\kappa \equiv \kappa^\perp$. Finally, f_{t_r} in Eq. (11) is a regularization function described in the next section. The subscript t_r is a cutoff parameter. For completeness, let us mention that terms \mathcal{H}_{A^4} and $\mathcal{H}_{[\partial A A]^2}$ give rise to Hamiltonian terms with four particle operators [18,19].

B. Effective Hamiltonians

The RGPEP introduces the concept of effective particles. Canonical operators are transformed into effective ones by means of a similarity transformation

$$a_t = \mathcal{U}_t a_0 \mathcal{U}_t^\dagger, \quad (13)$$

where \mathcal{U}_t is an anti-Hermitian operator and t the renormalization-group parameter, which can be related to s and λ by

$$s = 1/\lambda = t^{1/4}. \quad (14)$$

The parameter s has units of length and is associated with the *size* of effective particles; λ has units of mass and is associated with the energy *scale*. While bare operators $a_0^{(\dagger)}$ annihilate (create) bare, pointlike particles, effective particle operators $a_t^{(\dagger)}$ annihilate (create) particles of size s .

The RGPEP is based on the demand that

$$H_0(a_0) = H_t(a_t), \quad (15)$$

where H_t is the effective Hamiltonian. Denoting $\mathcal{H}_t = H_t(a_0)$ and differentiating Eq. (15), one can derive the RGPEP equation

$$\frac{d\mathcal{H}_t}{dt} = [[\mathcal{H}_f, \mathcal{H}_{Pt}], \mathcal{H}_t], \quad (16)$$

with the generator $\mathcal{G}_t = [\mathcal{H}_f, \mathcal{H}_{Pt}]$ defining the unitary transformation in Eq. (13). The operator \mathcal{H}_f is the Hamiltonian term that does not contain interactions [Eq. (10)]. The operator \mathcal{H}_{Pt} is identical to \mathcal{H}_t , but it contains a factor equal to $(\sum_i p_i^+)^2$, with i denoting all particles involved in the interaction [20]. Equation (16) can be solved order by order using a perturbative expansion of \mathcal{H}_t in powers of the coupling constant g :

$$\mathcal{H}_t = \mathcal{H}_0 + g\mathcal{H}_{t1} + g^2\mathcal{H}_{t2} + g^3\mathcal{H}_{t3} + g^4\mathcal{H}_{t4} + \dots \quad (17)$$

The description of the three-gluon vertex considered here involves powers not larger than third. Following the notation explained above Eq. (10), this requires terms of the type

$$\begin{aligned} \mathcal{H}_t = & \mathcal{H}_{11,0,t} + \mathcal{H}_{21,g,t} + \mathcal{H}_{12,g,t} + \mathcal{H}_{11,g^2,t} + \mathcal{H}_{22,g^2,t} \\ & + \mathcal{H}_{12,g^3,t} + \mathcal{H}_{21,g^3,t}, \end{aligned} \quad (18)$$

where an additional subscript indicates the power of the coupling constant each term contains. Introducing Eq. (18) in the RGPEP Eq. (16) yields products of Hamiltonians of different orders. The equation can be then solved order by order (see Appendix A). From all terms involved in third-order solutions, we will focus only on those relevant in the

calculation of the three-gluon vertex, namely, on the ones with two creation and one annihilation operators and vice versa.

C. Regularization and counterterms

The canonical Hamiltonian presents ultraviolet and small- x divergences that have to be treated through the RGPEP. Integration of the RGPEP equation yields exponential functions called form factors (cf. Appendix A):

$$f_{ab,t} = e^{-ab^2 t}, \quad (19)$$

where $ab := \mathcal{M}_a^2 - \mathcal{M}_b^2$ represents differences of invariant masses of particle configurations a and b associated, respectively, with all creation and annihilation operators in a vertex. For example, in a vertex $a_1^\dagger a_2^\dagger a_3$ (cf. Fig. 1), the form factor is

$$f_{t12,3} = \exp[-t(\mathcal{M}_{12}^2 - \mathcal{M}_3^2)^2], \quad (20)$$

with invariant masses defined as $\mathcal{M}_{i\dots j}^2 = (p_i + \dots + p_j)^2$. For single gluons $\mathcal{M}_i^2 = m_g^2$, and for pairs $\mathcal{M}_{ij}^2 = \frac{\kappa_{ij}^2 + m_g^2}{x_{i/p} x_{j/p}}$, where $x_{i/p} = x_i/x_p$ and $x_p = x_i + x_j$. Note that, in distinction to the previous work [19], \mathcal{M}_3^2 is not zero, and, thus, form factors change from

$$f_{ii,j,t} = \exp\left(-t \frac{\kappa_{ij}^4}{x_i^2 x_j^2}\right) \quad (21)$$

to

$$f_{ii,j,t} = \exp\left[-t \left(\frac{\kappa_{ij}^2 + m_g^2}{x_i x_j} - m_g^2\right)^2\right]. \quad (22)$$

These factors remove all ultraviolet divergences present in a single interaction term.

On the other hand, to tackle the more subtle small- x divergences appearing in loop integrals, we introduce a regulating function depending on a small cutoff t_r in each vertex:

$$f_{t_r,12,3} = \exp[-t_r(\mathcal{M}_{12}^2 - \mathcal{M}_3^2)^2]. \quad (23)$$

The behavior of form factors with and without a gluon mass is different around $\kappa_{ij} = 0$ and $x_i, x_j = 0$, precisely the region in which loop integrals diverge. The gluon mass and t_r remove all small- x divergences.

The result in the limit $t_r \rightarrow 0$ and $m_g \rightarrow 0$ must be then analyzed, and any possible remaining divergence should be canceled by counterterms.

Thus, the counterterms provide the initial condition of the differential equation (16) and are such that, in the limit in which the cutoffs are lifted, the canonical Hamiltonian

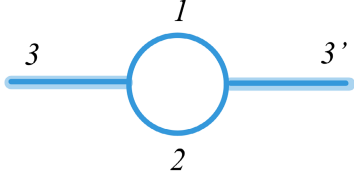


FIG. 2. Second-order self-energy diagram resulting from the product of two first-order three-gluon vertices (cf. Fig. 1). Thick lines represent effective gluons, and thin lines represent creation and annihilation operators that have been eliminated in the normal ordering.

must be recovered and any cutoff dependence must be removed. Therefore, the initial Hamiltonian consists of the (regularized) canonical Hamiltonian plus counterterms.

To illustrate the procedure in a simple case, consider the self-energy contribution resulting from the product of two first-order vertices (cf. Fig. 2):

$$\begin{aligned} \hat{\mu}_{t,ab}^2 &= 2 \sum_1 \int [1] \frac{1}{p_1^+} \\ &\times \left\{ \int [x\kappa] \frac{\kappa^2 P(x)}{2x(1-x)} \frac{f_{t+t_r}^2 - f_{t_r}^2}{\mathcal{M}^2 - m_g^2} \right\} a_1^\dagger a_1 + \hat{\mu}_{0,ab}^2, \end{aligned} \quad (24)$$

where $P(x)$ is the Altarelli-Parisi gluon splitting function [36].

Ultraviolet divergences are regularized by form factors f_t that suppress interactions with changes of invariant masses greater than about $\lambda = t^{-1/4}$. But terms that do not contain such functions may diverge, and a counterterm is required to cancel the cutoff dependence introduced by regulating functions. In Eq. (24), the counterterm is represented by $\hat{\mu}_{0,ab}^2$.

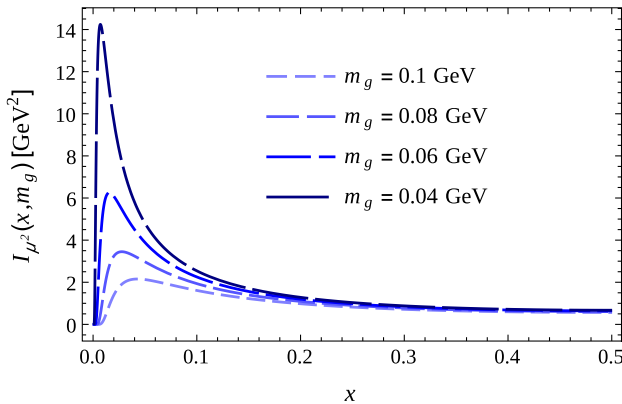


FIG. 3. Integrand of Eq. (26) after numerical integration over κ^\perp for different values of the parameter m_g . The gluon mass acts as a regulator: The smaller its value, the more the tendency to infinity of the integrand for x close to 0. The behavior is symmetric for $0.5 < x < 1$.

There are also small- x divergences that cannot be regulated by the RGPEP and that arise from *zero modes*. The presence of a gluon mass avoids the appearance of such infinities. On the other hand, the divergence of the self-energy due to small- x singularities is not a problem, because an isolated gluon is not a physical state, and, thus, its mass is not an observable.

The counterterm is

$$\begin{aligned} \hat{\mu}_{0,ab}^2 &= 2 \sum_1 \int [1] \frac{1}{p_1^+} \left\{ \int [x\kappa] \frac{\kappa^2 P(x)}{2x(1-x)} \frac{f_{t_r}^2}{\mathcal{M}^2 - m_g^2} \right. \\ &\left. + \mu_{0,m_g}^2 \right\} a_1^\dagger a_1, \end{aligned} \quad (25)$$

and the self-energy term can be finally written as

$$\begin{aligned} \hat{\mu}_{t,ab}^2 &= 2 \sum_1 \int [1] \frac{\mu_t^2}{p_1^+} a_1^\dagger a_1 \\ &= 2 \sum_1 \int [1] \frac{1}{p_1^+} \left[\int [x\kappa] \frac{\kappa^2 P(x)}{2x(1-x)} \frac{f_{t+t_r}^2}{\mathcal{M}^2 - m_g^2} \right. \\ &\left. + \mu_{0,m_g}^2 \right] a_1^\dagger a_1. \end{aligned} \quad (26)$$

The remaining dependence on t_r vanishes, because this parameter appears in addition to t in form factors [11]. In contrast, note that the gluon mass is still necessary to regulate small- x divergences, as it is shown in Fig. 3, where the integrand of Eq. (26) is plotted after numerical integration in κ^\perp for different values of the gluon-mass parameter m_g . Finally, μ_{0,m_g}^2 is an ultraviolet finite remnant that cannot be fixed by the RGPEP procedure alone, and, as the subscript m_g indicates, it can be divergent in the small- x limit and, thus, used to cancel the divergence on μ_t^2 , in case we need it to be finite [37].

Equation (26) can be integrated analytically in the limit of small mass m_g using the procedure described in Appendix B. After the integration, one can identify divergent and finite terms in the resulting expression:

$$\mu_t^2 = -\sqrt{\frac{\pi}{2}} \frac{1}{4\sqrt{t}} \left[\log(tm_g^4) + \log(8e^{\gamma_E}) + \frac{23}{6} \right] + \mu_{0,m_g}^2, \quad (27)$$

where γ_E is the Euler-Mascheroni constant. Note how clearly $\mu_t^2 \rightarrow \infty$ when $m_g \rightarrow 0$.

III. THREE-GLUON VERTEX AND RUNNING COUPLING

From the expansion of Eqs. (17) and (18), we identify the three-gluon-vertex structure in those terms that annihilate (create) one effective gluon and create (annihilate) two ones. Indeed, the expression (cf. Fig. 4)

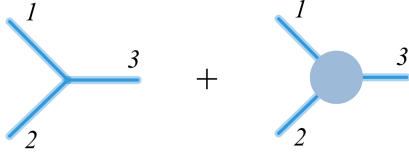


FIG. 4. Illustration of the three-gluon vertex as a sum of structures with annihilation of one and creation of two effective gluons. The first term is proportional to g , and the second one is proportional to g^3 . The latter is a sum of different structures represented in Fig. 5.

$$\begin{aligned} \mathcal{V}_{21t} &= g\mathcal{Y}_{21t} + g^3\mathcal{K}_{21t} \\ &= \sum_{123} \int [123] \tilde{\delta}(p^\dagger - p) f_{t,ab} \{g\tilde{\mathcal{Y}}_{21t} \\ &\quad + g^3(\tilde{\mathcal{K}}_{21t} + \tilde{\mathcal{K}}_{210})\} a_{t1}^\dagger a_{t2}^\dagger a_{t3} \end{aligned} \quad (28)$$

has first- and third-order terms.

The first-order term is given by Eq. (11) but including now the form factor f_t and with the additional difference that particle operators are of type t and have a width s . The third-order term is a sum of products of interactions that result from introducing Eq. (17) in Eq. (16) and its associated counterterm $\tilde{\mathcal{K}}_{210}$. We can distinguish ten different types of contributions depending on the operator product contained in them. They are represented diagrammatically in Fig. 5.

In terms of these diagrams, the third-order component in Eq. (28) is written as

$$\tilde{\mathcal{K}}_{21t} + \tilde{\mathcal{K}}_{210} = \frac{\sum_n \gamma_t(n)}{2 \cdot 16\pi^3} + \frac{\gamma_0(j)}{2 \cdot 16\pi^3}, \quad (29)$$

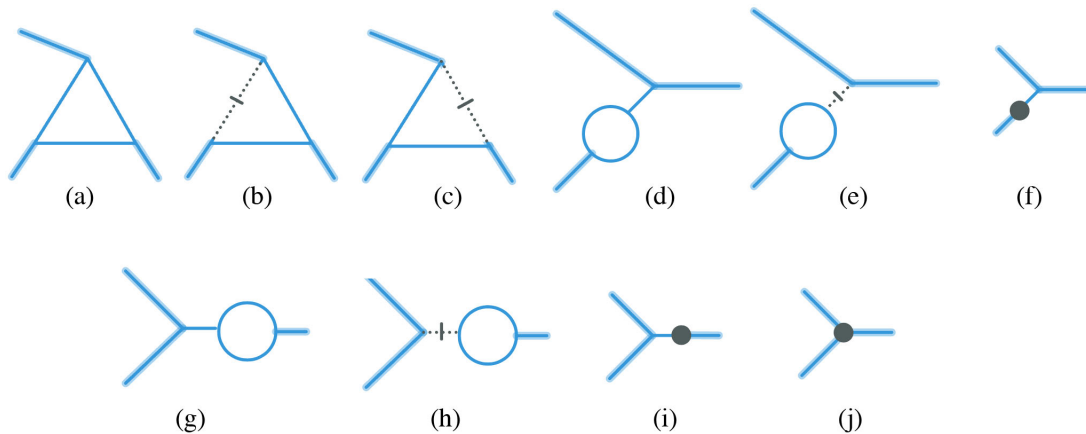


FIG. 5. Third-order diagrams resulting from products of first-order terms [diagrams (a), (d), and (g)] and from products of first-order times second-order terms [diagrams (b), (c), (e), (f), (h), and (i)]. The thick dots in (f) and (i) represent self-energy counterterms. Diagram (j) is the third-order counterterm that removes loop divergences arising at this order when the cutoff is lifted. Thicker lines represent effective creation and annihilation operators. Thin internal lines represent operators that are eliminated in the normal ordering. Dotted lines with a transverse dash indicate instantaneous interactions present in the canonical Hamiltonian due to the constraint Eq. (9).

where n ranges from a to i and j corresponds to the third-order counterterm, which is independent of t .

By inspection of the three-gluon vertex, the effective coupling depending on the RGPEP parameter t can be defined [18,19]. The running coupling is identified as the coefficient in front of the canonical color-, spin-, and momentum-dependent factor $Y_{123}(x_1, \kappa_{12}, \sigma)$ in the limit $\kappa_{12} \approx 0$ for some value of x_1 [18,19].

The coupling constant g_t must be set to a specific value g_0 at some arbitrary scale $t = t_0$ in agreement with experiments describing data using the effective Hamiltonian at $t = t_0$. Such a scale of reference can be introduced by means of the counterterm.

Recalling the procedure presented in Sec. II C, the third-order counterterm can be written as [19]

$$\tilde{\mathcal{K}}_{210} = \frac{1}{2 \cdot 16\pi^3} \left(-\sum_n \gamma_{t_0}(n) + \gamma_{\text{finite}} \right), \quad (30)$$

and contains terms that cancel all possible UV divergences, since the difference $\gamma_t(n) - \gamma_{t_0}(n)$ is ultraviolet finite regardless of the values of t and t_0 . Equation (29) can be expressed as

$$\tilde{\mathcal{K}}_{21t} + \tilde{\mathcal{K}}_{210} = \frac{1}{2 \cdot 16\pi^3} \left\{ \sum_n [\gamma_t(n) - \gamma_{t_0}(n)] + \gamma_{\text{finite}} \right\} \quad (31)$$

with the finite part γ_{finite} undetermined.

Similarly to the self-energy Hamiltonian term, μ_t^2 in Eq. (26), each $\gamma(n)$ involves three-dimensional loop integrals over the longitudinal momentum fractions x and relative transverse momenta κ^\perp of the internal virtual

particles. A detailed expression for the integrand of each of these structures can be found in [19], with the unique difference that in this work all invariant masses contain the canonical gluon mass m_g , which makes the integration procedure much more involved.

The approximation $\kappa_{12} \approx 0$ is now applied to both terms in Eq. (31). For the difference $\gamma_t(n) - \gamma_{t_0}(n)$, we have

$$\frac{\gamma_t(n) - \gamma_{t_0}(n)}{2 \cdot 16\pi^3} \approx [c_t(x_1) - c_{t_0}(x_1)] Y_{123}(x_1, \kappa_{12}, \sigma), \quad (32)$$

where the linear dependence on κ_{12} is contained in Y_{123} . For the finite part of the counterterm, which does not need to be specified here, we write

$$\gamma_{\text{finite}} \approx \tilde{c}_0(x_1, \kappa_{12}, \sigma), \quad (33)$$

with the function \tilde{c}_0 at most linear in κ_{12} .

Taking this into account, we can extract the running coupling from the three-gluon vertex at first order in κ_{12} , identifying the coefficient in front of the bare vertex structure Y_{123} :

$$\begin{aligned} \tilde{V}_{21t} &= g\tilde{\mathcal{Y}}_{21t} + g^3(\tilde{\mathcal{K}}_{21t} + \tilde{\mathcal{K}}_{210}) \\ &\approx \{g + g^3[c_t(x_1) - c_{t_0}(x_1)]\} Y_{123} + \tilde{c}_0(x_1, \kappa_{12}, \sigma) \\ &\quad + \mathcal{O}(\kappa_{12}^2, g^4). \end{aligned} \quad (34)$$

The running coupling at third order is, thus,

$$g_t \equiv g + g^3[c_t(x_1) - c_{t_0}(x_1)], \quad (35)$$

and, setting g_t to be g_0 at the scale t_0 , we are left with

$$g_t = g_0 + g_0^3(c_t(x_1) - c_{t_0}(x_1)). \quad (36)$$

A. Term a

The triangle term (a) gathers products of three first-order vertices Eq. (10):

$$\begin{aligned} &(\tilde{\mathcal{K}}_{21t}(x_1, \kappa_{12}, \sigma) + \tilde{\mathcal{K}}_{210}(x_1, \kappa_{12}, \sigma))|_a \\ &= \mathcal{Y}_{0,ax} \mathcal{Y}_{0,xy} \mathcal{Y}_{0,yb} (C_{t,axyb} - C_{t_0,axyb}), \end{aligned} \quad (37)$$

where the contribution of the third-order counterterm is included. $\mathcal{Y}_{0,a\beta}$ are first-order interaction vertices from the initial Hamiltonian, with subscripts denoting particle configurations before and after each interaction. The RGPEP factor $C_{t,axyb}$ results from solving the RGPEP equations, and it is made of functions of invariant masses and form factors (see Appendix A, Fig. 8, and Refs. [19,20]).

The product of first-order vertices Eq. (11) that leads to diagram (a) is

$$\mathcal{Y}_{0,ax} \mathcal{Y}_{0,xy} \mathcal{Y}_{0,yb} = 8 \sum_{123} \int [123] \int \frac{dx d^2\kappa}{16\pi^3} \frac{f_{t_r,ax} f_{t_r,xy} f_{t_r,yb}}{p_3^{+2}} \frac{\sum_{678} Y_{682}^* Y_{167} Y_{783}}{(x-x_1)(1-x)x} \delta(p_7 + p_8 - p_3) a_1^\dagger a_2^\dagger a_3, \quad (38)$$

where the numbers 6, 7, and 8 label intermediate gluons. The contribution of this diagram is

$$\gamma_t(a) - \gamma_{t_0}(a) = 4iN_c Y_{123} f^{c_1 c_2 c_3} \int_{x_1}^1 \frac{dx \epsilon^{ijk}(a)}{(x-x_1)(1-x)x} \int d^2\kappa f_{t_r,ax} f_{t_r,xy} f_{t_r,yb} \kappa_{68}^i \kappa_{16}^j \kappa^k \frac{C_{t,axyb} - C_{t_0,axyb}}{p_3^{+2}} + (1 \leftrightarrow 2), \quad (39)$$

where $\epsilon^{ijk}(a)$ is a structure that depends on the relative transverse momentum of external gluons κ_{12}^\perp and emerges from the product of polarizations:

$$\sum_{678} Y_{682}^* Y_{167} Y_{783} = \frac{N_c}{2} i f^{c_1 c_2 c_3} \kappa_{68}^i \kappa_{16}^j \kappa^k \epsilon^{ijk}(a). \quad (40)$$

In order to evaluate Eq. (39), we simplify the integrand proceeding as described in Appendix B. The integration over x is divided into regions called **I**, **II**, and **III**: $(x_1, x_1 + \bar{m}_g)$, $(x_1 + \bar{m}_g, 1 - \bar{m}_g)$, and $(1 - \bar{m}_g, \bar{m}_g)$, respectively, where \bar{m}_g is dimensionless and depends on m_g . The integral over x diverges in regions **I** and **III** but is finite in region **II**.

(i) **Region II**.—Since there is no divergence in this interval, limits $m_g \rightarrow 0$ and $t_r \rightarrow 0$ can be applied, and the result is analogous to the one obtained in [19].

(ii) **Regions I and III**.—The first and third intervals are evaluated separately by expanding the integrals over $x \approx x_1$ and $x \approx 1$, respectively, and keeping only the dominant powers. Then, an expansion around $\kappa_{12} \approx 0$ is applied, yielding an expression proportional to the structure Y_{123} ; cf. Eq. (32) with integrals that can be evaluated analytically.

The total contribution of diagram (a) is obtained after adding the result from each interval. A logarithmic dependence on the gluon mass parameter m_g remains:

$$\begin{aligned} \gamma_t(a) - \gamma_{t_0}(a) &\rightarrow N_c Y_{123} \pi \log\left(\frac{t}{t_0}\right) \left[-\frac{11}{3} + \frac{1}{6} h_a(x_1)\right] \\ &\quad - \frac{16\pi N_c Y_{123}}{x_1 x_2} \frac{\bar{t} - \bar{t}_0}{x_1^2 + x_2^2} \frac{\bar{m}_g}{\bar{t}_r}, \end{aligned} \quad (41)$$

where

$$\begin{aligned} \frac{1}{6} h_a(x_1) &= -3 \log(\bar{m}_g^4 \sqrt{\bar{t}_1} e^{\gamma_E}) - 5 - \log(2) \\ &\quad + \frac{1 - x_1^2 x_2^2}{(1 + x_1^2)(1 + x_2^2)} - \frac{2}{1 - x_2^2} \log\left(\frac{1 + x_2^2}{x_1 x_2}\right) \\ &\quad - \frac{2}{1 - x_1^2} \log\left(\frac{1 + x_1^2}{x_1 x_2}\right) + \left(1 - \frac{1}{1 - x_1^2} - \frac{1}{1 - x_2^2}\right) \\ &\quad \times \log\left[\frac{(x_1^2 + x_2^2)x_1^2 x_2^2}{2(1 + x_2^2)(1 + x_1^2)}\right], \end{aligned} \quad (42)$$

γ_E being the Euler-Mascheroni constant.

B. Terms (b)–(i)

Terms (b) and (c) are products of the first-order vertex and the second-order canonical interaction. For the term (b), we have

$$\gamma_t(b) - \gamma_{t_0}(b) \rightarrow \frac{16\pi N_c Y_{123}}{x_0 x_2} \frac{(\bar{t} - \bar{t}_0)}{x_1^2 + x_2^2} \frac{\bar{m}_g}{\bar{t}_r}. \quad (43)$$

This contribution exactly cancels the term proportional to $\bar{t} - \bar{t}_0$ in Eq. (41).

The contribution of (c) turns out to be negligible in the limit $m_g, t_r \rightarrow 0$.

Terms (e) and (h) also result from the product of the same kind of interactions as (b) and (c). They do not contribute to the running coupling due to the absence of linear terms in κ_{12} that could give rise to the canonical polarization structure Y_{123} of Eq. (11).

Terms (d) and (f) are also obtained from products of first-order interactions, two of them forming a second-order self-energy contribution $\hat{\mu}_t$. Thus, diagrams (d) and (f) come from the first and second terms in Eq. (26), respectively, the latter containing the counterterm. Their sum gives the following result:

$$\begin{aligned} \gamma_t(d+f) - \gamma_{t_0}(d+f) \\ \rightarrow \pi N_c Y_{123} \log\left(\frac{t}{t_0}\right) \left[\frac{11}{3} + \frac{1}{6} h_{d+f}(x_1)\right], \end{aligned} \quad (44)$$

where

$$\begin{aligned} \frac{1}{6} h_{d+f}(x_1) &= 2 \log(e^{\gamma_E} \bar{m}_g^4 \sqrt{\bar{t} \bar{t}_0}) + 2 \log 2 + 4 \\ &\quad - 2 \frac{x_2^2}{1 - x_2^2} \log\left(\frac{1 + x_2^2}{2x_2^2}\right) \\ &\quad - 2 \frac{x_1^2}{1 - x_1^2} \log\left(\frac{1 + x_1^2}{2x_1^2}\right). \end{aligned} \quad (45)$$

Terms (g) and (i) are analogous, but the loop is located in another leg of the diagram:

$$\begin{aligned} \gamma_t(g+i) - \gamma_{t_0}(g+i) \\ \rightarrow \frac{\pi N_c Y_{123}}{6} \log\left(\frac{t}{t_0}\right) [11 + h_{g+i}(x_1)] \end{aligned} \quad (46)$$

with

$$\frac{1}{6} h_{g+i}(x_1) = \log(e^{\gamma_E} \bar{m}_g^4 \sqrt{\bar{t} \bar{t}_0}) + \log 2 + 1. \quad (47)$$

The final expression of the running coupling is given by Eqs. (41)–(47):

$$g_\lambda = g_0 - N_c \frac{g_0^3}{48\pi^2} \log\left(\frac{\lambda}{\lambda_0}\right) [11 + h(x_1)], \quad (48)$$

with $\lambda = 1/\sqrt{4t}$ and

$$\begin{aligned} h(x_1) &= -6 \left\{ \frac{1 + x_2^2}{1 - x_2^2} \log\left[\frac{(1 + x_2^2)^2}{x_2^2}\right] \right. \\ &\quad + \frac{1 + x_1^2}{1 - x_1^2} \log\left[\frac{(1 + x_1^2)^2}{x_1^2}\right] - \frac{1 - x_1^2 x_2^2}{(1 + x_1^2)(1 + x_2^2)} \\ &\quad \left. + \left(1 - \frac{1}{1 - x_1^2} - \frac{1}{1 - x_2^2}\right) \log\left[\frac{8(1 + x_2^2)(1 + x_1^2)}{(x_1^2 + x_2^2)}\right] \right\}. \end{aligned} \quad (49)$$

As one can see, the obtained running coupling does not contain any explicit dependence on cutoff t_r or on the gluon mass m_g . All possible dependencies have been canceled after adding the contributions. Thus, the final result is finite and independent of m_g in the limit $m_g \rightarrow 0$, even when the contributions diverge individually in this limit; cf. Fig. 6.

C. Analysis of results

It is interesting to observe the results shown in Fig. 7. The 2D plot shows separate contributions to the running coupling (for $x_1 = 0.5$) coming from different diagrams in Fig. 5. Contributions (d) + (f) and (g) + (i) are decreasing and, therefore, asymptotically free, whereas contribution (a) is increasing. All three contributions balance out, and their sum is extremely close to the value of the running coupling obtained from standard calculations using Feynman diagrams (bold black line). The difference is

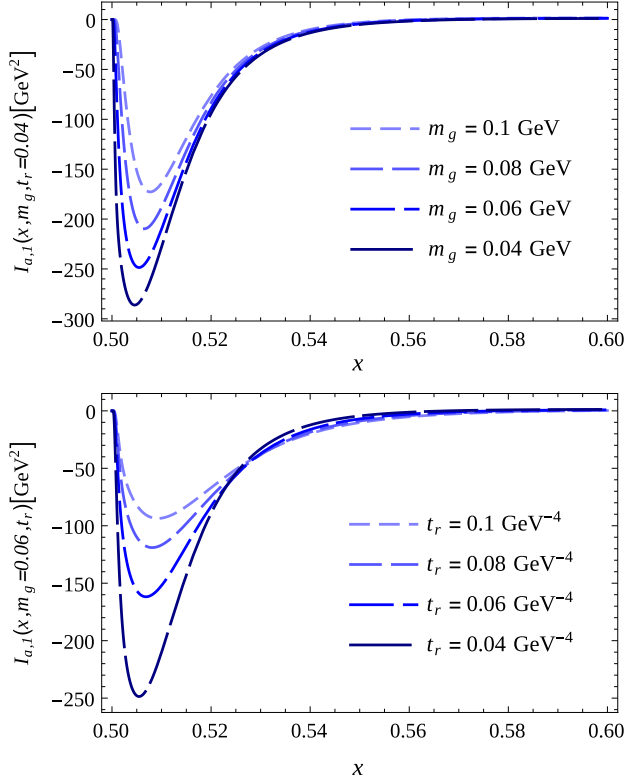


FIG. 6. Result of integration over κ^\perp for region **I** of term $\gamma(a)$ (see Appendix B). In the upper panel, t_r is fixed to 0.04 GeV^{-4} , while in the bottom panel, m_g is fixed to 0.06 GeV . In both figures, $t = 2 \text{ GeV}^{-4}$, $t_0 = 1 \text{ GeV}^{-4}$, and $x_1 = 0.5$. Divergences occur either when $t_r \rightarrow 0$ or $m_g \rightarrow 0$.

due to the appearance of function $h(x_1)$ in Eq. (48), which for the considered value $h(0.5) = -0.863$. This small difference does not even reach a maximum of 2% in the treated range of scale λ .

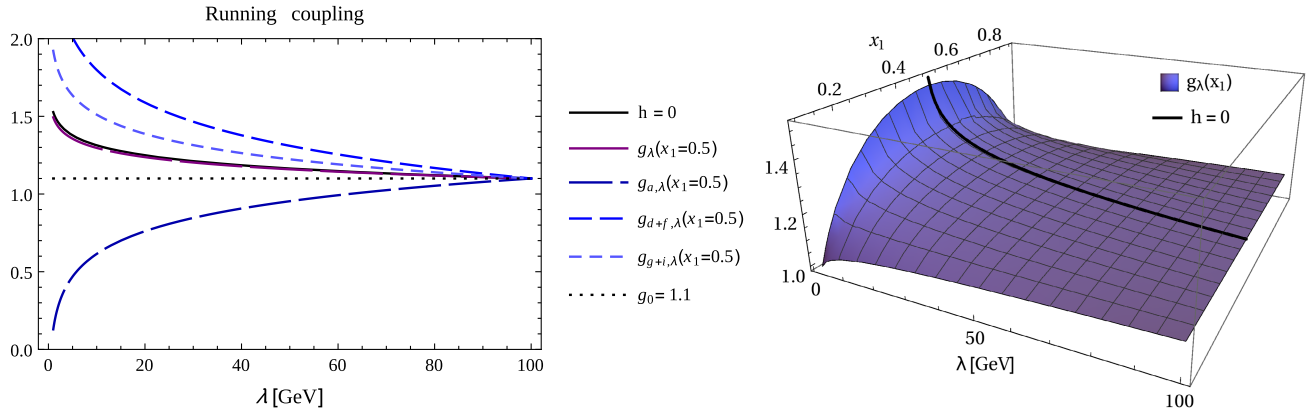


FIG. 7. Left: The resulting running coupling Eq. (48) varying with λ for $x_1 = 0.5$ (purple). It results from the sum of the contributions coming from the different diagrams (blue dashed lines). It appears very close to the running coupling result corresponding to $h(x_1) = 0$ (bold black line) (cf. Refs. [18,19]). Right: The function $g_\lambda(x_1)$ shows a dependence on x_1 due to the function $h(x_1)$ appearing in Eq. (49), differing from the case $h(x_1) = 0$ as x_1 approaches the ends $x_1 = 1$ and $x_1 = 0$. The difference is more pronounced for lower values of λ .

Such a difference grows, however, for values of x_1 that distance from the central one $x_1 = 0.5$, reaching a maximum at $x_1 = 0$ and $x_1 = 1$, as is plotted in the curved surface of the 3D Fig. 7. It seems reasonable to define the running coupling at $x_1 = 0.5$. Yet, a need for a more adequate definition of the running of the coupling and including higher-order Hamiltonians than third is not discarded.

The difference in sign in the variation of the coupling provided by the different pieces represented in Fig. 5 resembles the difference in sign of terms in the effective potential obtained for quarks in the bound-state problem [9,33]. In the bound-state equation, self-energy interactions are repulsive, while the exchange of gluons between quarks is attractive. Hence, attractive and repulsive forces combine to form bound states, canceling divergences that appear in them when they are taken separately. It is not surprising then that Hamiltonian terms combine analogously in the three-gluon vertex, too. Indeed, terms $(d) + (f)$ and $(g) + (i)$ are self-energy Hamiltonians multiplied by a three-gluon vertex, whereas term (a) can be seen as a gluon exchange term that is contracted with a three-gluon vertex. In other words, the first case is a three-gluon vertex with one of the gluons interacting with itself, whereas in the latter case, one gluon splits in two, which, in turn, exchange another gluon.

It is not trivial how the cutoff dependence appearing in different diagrams cancels each other exactly in the limit $m_g \rightarrow 0$. The running coupling is, in fact, insensitive to the gluon mass and cutoff, as long as they are sufficiently small. Yet, the presence of the mass is indispensable for the cancellation of divergences. The fact that the function $h(x_1)$ appears and that it is different from the functions h obtained in the old version of the calculation [19] evidences the finite dependence on the regularization procedure, which needs to be clarified and better understood in a deeper analysis.

IV. SUMMARY AND CONCLUSIONS

We have analyzed the effect of a new regularization with canonical gluon mass in the front-form Hamiltonian within the RGPEP. Following previous studies, we have derived the three-gluon-vertex effective Hamiltonian term in a third-order expansion in powers of the coupling constant. The inclusion of a gluon mass provides a suitable regularization procedure for small- x divergences. The presence of the mass makes regularization factors go to zero faster than any positive power of x as $x \rightarrow 0$.

We have computed the running of the coupling constant using the coefficient function in front of the three-gluon-vertex structure in the approximation $\kappa_{12}^{\perp} \approx 0$, describing the running of the coupling by its variation with the energy scale.

Although the new regularization procedure differs conceptually from the one employed in previous calculations, it leads to a similar type of function, exhibiting asymptotic freedom. The running of the coupling depends on the renormalization-group parameter λ in the same way as the running coupling calculated using Feynman diagrams for off-shell Green's functions depends on momentum, even though both approaches are fairly different.

In our definition of the running coupling, all terms depending on m_g cancel out in a nontrivial way for infinitesimally small gluon mass. Hence, there is no dependence on the mass parameter m_g or on the cutoff t_r , even though separate contributions diverge in this limit.

As in the foregoing studies, a finite dependence on the regularization remains, which is manifest in the appearance of the function $h(x_1)$ in Eq. (48). For $x_1 = 0.5$, the running coupling has values extremely close to the one provided by standard calculations [and would be identical for $h(x_1) = 0$], with less than a 2% difference within the entire range of the scale λ considered. In contrast to the previous calculation, the dependence on x_1 appears not only in contribution (a) [Eq. (41)], but also in (d) + (f) [Eq. (44)]. Removal of such finite dependence requires a deeper understanding of how to define the running coupling constant in Hamiltonians and, eventually, a higher-order analysis. The inclusion of longitudinal polarization for gluon with mass ought to be considered [38].

ACKNOWLEDGMENTS

We thank Stanisław D. Głazek for helpful discussions and acknowledge financial support from the FEDER funds, Project Ref. No. A-FQM-406-UGR20, from MCIN/AEI/10.13039/501100011033, Projects Ref. No. PID2020-114767GB-I00, No. PID2019-108655GB-I00, and No. PID2019-106080GB-C21, and FPU21/04180 grant from the Spanish Ministry of Universities.

APPENDIX A: SOLUTIONS ORDER BY ORDER

This appendix summarizes the main steps for systematically solving the RGPEP equation (16) perturbatively.

The reader interested in a deeper discussion may consult Ref. [20]. The effective Hamiltonian is a solution to the RGPEP equation:

$$\mathcal{H}'_t = [[\mathcal{H}_f, \mathcal{H}_{P_t}], \mathcal{H}_t]. \quad (\text{A1})$$

The operator \mathcal{H}_{P_t} is defined in terms of the effective Hamiltonian \mathcal{H}_t , differing in a factor $(\frac{1}{2} \sum_i p_i^+)^2$, with i denoting the particles involved in an interaction [20].

The perturbative solution is given as a power expansion in the coupling constant g :

$$\mathcal{H}_t = \mathcal{H}_0 + g\mathcal{H}_{t1} + g^2\mathcal{H}_{t2} + g^3\mathcal{H}_{t3} + g^4\mathcal{H}_{t4} + \dots \quad (\text{A2})$$

For instance, in a fourth-order expansion, one has

$$\begin{aligned} \mathcal{H}'_0 + g\mathcal{H}'_{t1} + g^2\mathcal{H}'_{t2} + g^3\mathcal{H}'_{t3} + g^4\mathcal{H}'_{t4} \\ = [[\mathcal{H}_0, \mathcal{H}_0 + g\mathcal{H}_{1P_t} + g^2\mathcal{H}_{2P_t} + g^3\mathcal{H}_{3P_t} + g^4\mathcal{H}_{4P_t}], \\ \mathcal{H}_0 + g\mathcal{H}_{t1} + g^2\mathcal{H}_{t2} + g^3\mathcal{H}_{t3} + g^4\mathcal{H}_{t4}], \end{aligned} \quad (\text{A3})$$

which can be solved order by order:

$$\mathcal{H}'_0 = 0, \quad (\text{A4})$$

$$g\mathcal{H}'_{t1} = [[\mathcal{H}_0, g\mathcal{H}_{1P_t}], \mathcal{H}_0], \quad (\text{A5})$$

$$g^2\mathcal{H}'_{t2} = [[\mathcal{H}_0, g^2\mathcal{H}_{2P_t}], \mathcal{H}_0] + [[\mathcal{H}_0, g\mathcal{H}_{1P_t}], g\mathcal{H}_{t1}], \quad (\text{A6})$$

$$\begin{aligned} g^3\mathcal{H}'_{t3} = [[\mathcal{H}_0, g^3\mathcal{H}_{3P_t}], \mathcal{H}_0] + [[\mathcal{H}_0, g^2\mathcal{H}_{2P_t}], g\mathcal{H}_{t1}] \\ + [[\mathcal{H}_0, g\mathcal{H}_{1P_t}], g^2\mathcal{H}_{t2}], \end{aligned} \quad (\text{A7})$$

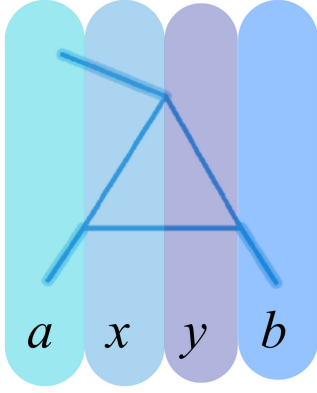
$$\begin{aligned} g^4\mathcal{H}'_{t4} = [[\mathcal{H}_0, g^4\mathcal{H}_{4P_t}], \mathcal{H}_0] + [[\mathcal{H}_0, g^3\mathcal{H}_{3P_t}], g\mathcal{H}_{t1}] \\ + [[\mathcal{H}_0, g^2\mathcal{H}_{2P_t}], g^2\mathcal{H}_{t2}] + [[\mathcal{H}_0, g\mathcal{H}_{1P_t}], g^3\mathcal{H}_{t3}]. \end{aligned} \quad (\text{A8})$$

We present solutions to these equations in terms of matrix elements $\mathcal{H}_{tab} = \langle a | \mathcal{H} | b \rangle$:

$$\mathcal{H}_{t1ab} = f_{tab} \mathcal{H}_{01ab}, \quad (\text{A9})$$

$$\mathcal{H}_{t2ab} = f_{tab} \sum_x \mathcal{H}_{01ax} \mathcal{H}_{01xb} \mathcal{B}_{taxb} + f_{tab} \mathcal{G}_{02ab}, \quad (\text{A10})$$

$$\begin{aligned} \mathcal{H}_{t3ab} = f_{tab} \mathcal{G}_{03ab} + f_{tab} \sum_{xy} \mathcal{H}_{01ax} \mathcal{H}_{01xy} \mathcal{H}_{01yb} \mathcal{C}_{taxyb} \\ + f_{tab} \sum_x (\mathcal{H}_{01ax} \mathcal{G}_{02xb} + \mathcal{G}_{02ax} \mathcal{H}_{01xb}) \mathcal{B}_{taxb}, \end{aligned} \quad (\text{A11})$$


 FIG. 8. Particle configurations a , x , y , and b in diagram (a).

$$\begin{aligned}
 \mathcal{H}_{t4ab} = & f_{tab} \sum_{xyz} \mathcal{H}_{01ax} \mathcal{H}_{01xy} \mathcal{H}_{01yz} \mathcal{H}_{01zb} \mathcal{D}_{taxyzb} \\
 & + f_{\tau ab} \sum_{xy} (\mathcal{H}_{01ax} \mathcal{H}_{01xy} \mathcal{G}_{02yb} + \mathcal{H}_{01ax} \mathcal{G}_{02xy} \mathcal{H}_{01yb} \\
 & + \mathcal{G}_{02ax} \mathcal{H}_{01xy} \mathcal{H}_{01yb}) \mathcal{C}_{taxyb} \\
 & + f_{\tau ab} \sum_x (\mathcal{G}_{02ax} \mathcal{G}_{02xb} + \mathcal{H}_{01ax} \mathcal{G}_{03xb} \\
 & + \mathcal{G}_{03ax} \mathcal{H}_{01xb}) \mathcal{B}_{taxb} + f_{\tau ab} \mathcal{G}_{04ab}, \quad (\text{A12})
 \end{aligned}$$

where operators \mathcal{G}_{02} , \mathcal{G}_{03} , and \mathcal{G}_{04} are the initial condition, being canonical terms or counterterms of the respective order [20]. The so-called RGPEP factors are given by

$$\mathcal{A}_{taxb} = [axp_{ax} + bxp_{bx}] f_{tab}^{-1} f_{tax} f_{tbx}, \quad (\text{A13})$$

$$\mathcal{B}_{taxb} = \int_0^t \mathcal{A}_{taxb} d\tau, \quad (\text{A14})$$

$$\mathcal{C}_{taxyb} = \int_0^t [\mathcal{A}_{\tau axb} \mathcal{B}_{\tau xyb} + \mathcal{A}_{\tau ayb} \mathcal{B}_{\tau axy}] d\tau, \quad (\text{A15})$$

$$\mathcal{D}_{taxyb} = \int_0^t [\mathcal{A}_{\tau axb} \mathcal{C}_{\tau xyzb} + \mathcal{A}_{\tau azb} \mathcal{C}_{\tau axyz} + \mathcal{A}_{\tau ayb} \mathcal{B}_{\tau axy} \mathcal{B}_{\tau yzb}], \quad (\text{A16})$$

with $f_{tab} := \exp[-ab^2 t]$ and $ab := \mathcal{M}_{ab}^2 - \mathcal{M}_{ba}^2$.

The subscripts a , b , x , and y represent particle configurations; cf. Fig. 8 and Ref. [20]. In this paper, we consider solutions up to third order.

APPENDIX B: INTEGRATION PROCEDURE

In this appendix, a systematic procedure to integrate expressions such as Eq. (39) is discussed. After introduction of the scale t_0 , integrals involved have the structure

$$\lim_{m_g \rightarrow 0} \int_{1-x_p}^1 dx \int_0^\infty d^2 \kappa^\perp \tilde{f}_{t_r} (f_{t,i} - f_{t_0,i}) C_i(x, x_1, \kappa, \kappa_{12}, m_g), \quad (\text{B1})$$

where \tilde{f}_{t_r} is the product of regularization form factors introduced at each interaction vertex and $(f_{t,i} - f_{t_0,i}) C_i$ denotes a sum of differences of form factors, evaluated at t and t_0 , multiplied by fractions depending on invariant masses [see $\mathcal{B}_{t(a)}$ in Eq. (C15) in [19], where the counterterm has not been taken into account yet]. $1 - x_p$ denotes the minimal momentum fraction carried in internal loops. In this work, it is equal to 1 or x_2 .

The limit $m_g \rightarrow 0$ is used to simplify the integrand. First, we introduce dimensionless variables using an arbitrary scale t_N :

$$\bar{t} = \frac{t}{t_N}, \quad \bar{\kappa}^\perp = \kappa^\perp t_N^{1/4}, \quad \bar{m}_g = m_g t_N^{1/4}. \quad (\text{B2})$$

After this change of variables, the behavior of the integrand in the neighborhood of $\kappa = 0$ and $x = 1$ or $x = 1 - x_p$ is studied. Form factors are decreasing exponentials of differences of invariant masses:

$$f_t = \exp[-t(\mathcal{M}^2 - m_g^2)^2], \quad (\text{B3})$$

with \mathcal{M} depending on $\bar{\kappa}$, \bar{m}_g , and x in the following way:

$$\mathcal{M}^2 = x_p^2 \frac{\bar{\kappa}^2 + \bar{m}_g^2}{(1-x)(x - (1-x_p))}. \quad (\text{B4})$$

There are two scales settled by \bar{m}_g and $\bar{\kappa}$; one corresponds to $\bar{\kappa} \gg \bar{m}_g$, in which the mass parameter can be ignored, and the other to $\bar{\kappa} \approx 0$, for which \bar{m}_g provides the necessary regularization when x is close to of $1 - x_p$ or 1. Thus, the limit $\bar{m}_g \rightarrow 0$ cannot be applied inside the integral, as it cuts off the divergences of invariant masses that take place when $x - (1 - x_p) < \bar{m}_g$ or $1 - x < \bar{m}_g$ if $\bar{\kappa} = 0$, necessary to regulate (B1).

If the integral over x is divided in three regions,

- (i) region **I**: $x \in (1 - x_p, (1 - x_p) + \bar{m}_g)$,
- (ii) region **II**: $x \in ((1 - x_p) + \bar{m}_g, 1 - \bar{m}_g)$, and
- (iii) region **III**: $x \in (1 - \bar{m}_g, 1)$,

it can be greatly simplified in intervals **I** and **III** applying approximations $1 - x \approx x_p$ and $x - (1 - x_p) \approx x_p$ respectively. The limit $\bar{m}_g \rightarrow 0$ can be safely applied in region **II**, since numerators of invariant masses are quadratic in \bar{m}_g , whereas denominators are linear in \bar{m}_g .

For example, in the self-energy integral Eq. (26), the three regions are

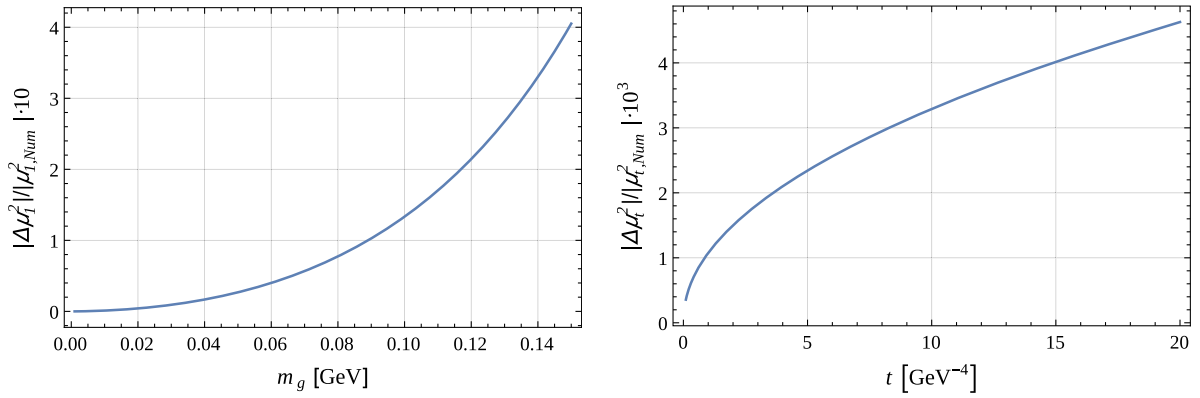


FIG. 9. Numerical check of the approximation taken in the integral of Eq. (26). The difference $\Delta\mu_t^2 = \mu_{t,\text{Num}}^2 - \mu_{t,\text{App}}^2$ normalized to the value of the numerical integration $\mu_{t,\text{Num}}^2$ is plotted as function of m_g for fixed t and vice versa: In the left figure, $t = 1 \text{ GeV}^{-4}$ and m_g goes from 10^{-3} to 0.15 GeV ; in the right plot, $m_g = 0.01 \text{ GeV}$ and t goes from 0.1 to 20 GeV^{-4} . The result is exact in the limit $m_g \rightarrow 0$.

$$\int_0^1 dx \rightarrow \lim_{\bar{m}_g \rightarrow 0} \left[\int_0^{\bar{m}_g} dx + \int_{\bar{m}_g}^{1-\bar{m}_g} dx + \int_{1-\bar{m}_g}^1 dx \right]. \quad (\text{B5})$$

The contribution in region **I** is obtained using the approximation $1 - x \approx 1$:

$$\mu_{t|\text{I}} = \frac{N_c}{(2\pi)^2} \int_0^{\bar{m}_g} \frac{dx}{x^2} \int d\bar{k} \frac{\bar{k}^3}{\bar{m}_g^2 + \bar{k}^2} \exp \left[-2\bar{t} \frac{(\bar{m}_g^2 + \bar{k}^2)^2}{x^2} \right], \quad (\text{B6})$$

that can be easily integrated:

$$\mu_{t|\text{I}} = -\frac{N_c}{(2\pi)^2} \sqrt{\frac{\pi}{2}} \frac{1}{8\sqrt{\bar{t}}} \left[2 + \gamma_E + 3 \log(2) + \log(tm_g^4) - \frac{1}{2} \log(tm_g^4) \right]. \quad (\text{B7})$$

In region **III**, the change of variables $y = 1 - x$ makes the integral analogous to the one on interval region **I** and the result is the same. In region **II**, the regularization can be safely lifted by taking the limit $t_r \rightarrow 0$ and $m_g \rightarrow 0$, yielding

$$\begin{aligned} \mu_{t|\text{II}} &= \frac{N_c}{(2\pi)^2} \int_{\bar{m}_g}^{1-\bar{m}_g} dx \int d\kappa \kappa \left[1 + \frac{1}{x^2} + \frac{1}{(1-x)^2} \right] \\ &\quad \times \exp \left[-2t \frac{\kappa^4}{x^2(1-x)^2} \right] \\ &= -\frac{N_c}{(2\pi)^2} \sqrt{\frac{\pi}{2}} \frac{1}{8\sqrt{t}} \left[\log(t_N m_g^4) + \frac{11}{3} \right]. \end{aligned} \quad (\text{B8})$$

Adding the results of the three intervals, one obtains Eq. (27). The dependence on the arbitrary scale t_N cancels and a logarithmic dependence on m_g is left as a remnant of the regulated divergence.

The error induced by this approximation is negligible in the limit of infinitesimally small gluon mass. This is shown in Fig. 9: The left panel shows the difference between the result obtained applying this procedure and the numerical integral, as a function of the gluon mass parameter m_g . The right panel shows the difference between the approximated analytical integral and the numerical one for different values of t and a fixed mass $m_g = 0.01 \text{ MeV}$. We recall that we are interested in the limit $m_g \rightarrow 0$.

[1] D. J. Gross and F. Wilczek, *Phys. Rev. Lett.* **30**, 1343 (1973).
 [2] D. J. Gross and F. Wilczek, *Phys. Rev. D* **9**, 980 (1974).
 [3] H. D. Politzer, *Phys. Rep.* **14**, 129 (1974).
 [4] H. D. Politzer, *Phys. Rev. Lett.* **30**, 1346 (1973).
 [5] R. P. Feynman, *Phys. Rev. Lett.* **23**, 1415 (1969).
 [6] S. D. Glazek and K. G. Wilson, *Phys. Rev. D* **48**, 5863 (1993).

[7] S. D. Glazek, *Acta Phys. Pol. B* **29**, 1979 (1997), <https://www.actaphys.uj.edu.pl/R/29/8/1979>.
 [8] P. A. M. Dirac, *Rev. Mod. Phys.* **21**, 392 (1949).
 [9] S. D. Glazek and A. P. Trawiński, *Few-Body Syst.* **58**, 49 (2017).
 [10] S. D. Glazek, *Phys. Rev. D* **90**, 045020 (2014).
 [11] S. D. Glazek, *Phys. Rev. D* **101**, 034005 (2020).
 [12] S. D. Glazek, *Phys. Rev. D* **103**, 014021 (2021).
 [13] M. Gómez-Rocha, *Few-Body Syst.* **58**, 65 (2017).

- [14] S. D. Glazek, M. Gómez-Rocha, J. More, and K. Serafin, *Phys. Lett. B* **773**, 172 (2017).
- [15] K. Serafin, M. Gómez-Rocha, J. More, and S. D. Glazek, *Eur. Phys. J. C* **78**, 964 (2018).
- [16] S. D. Glazek, *Phys. Rev. D* **85**, 125018 (2012).
- [17] S. D. Glazek, *Phys. Rev. D* **87**, 125032 (2013).
- [18] S. D. Glazek, *Phys. Rev. D* **63**, 116006 (2001).
- [19] M. Gómez-Rocha and S. D. Glazek, *Phys. Rev. D* **92**, 065005 (2015).
- [20] S. D. Glazek, *Acta Phys. Pol. B* **43**, 1843 (2012).
- [21] S. D. Glazek, *Acta Phys. Pol. B* **50**, 5 (2019).
- [22] M. Peláez, U. Reinoso, J. Serreau, M. Tissier, and N. Wschebor, *Rep. Prog. Phys.* **84**, 124202 (2021).
- [23] M. Peláez, U. Reinoso, J. Serreau, and N. Wschebor, *Phys. Rev. D* **107**, 054025 (2023).
- [24] M. Tissier and N. Wschebor, *Phys. Rev. D* **82**, 101701 (2010).
- [25] J. M. Cornwall, *Phys. Rev. D* **26**, 1453 (1982).
- [26] J. M. Cornwall, *Phys. Rev. D* **93**, 025021 (2016).
- [27] C. W. Bernard, *Nucl. Phys.* **B219**, 341 (1983).
- [28] C. W. Bernard, *Phys. Lett.* **108B**, 431 (1982).
- [29] A. C. Aguilar, M. N. Ferreira, and J. Papavassiliou, *Phys. Rev. D* **105**, 014030 (2022).
- [30] A. C. Aguilar, F. De Soto, M. N. Ferreira, J. Papavassiliou, F. Pinto-Gómez, C. D. Roberts, and J. Rodríguez-Quintero, *Phys. Lett. B* **841**, 137906 (2023).
- [31] A. C. Aguilar, D. Binosi, and J. Papavassiliou, *Phys. Rev. D* **95**, 034017 (2017).
- [32] D. Binosi and J. Papavassiliou, *Phys. Rev. D* **97**, 054029 (2018).
- [33] K. Serafin, M. Gómez-Rocha, J. More, and S. D. Glazek, *arXiv:2310.00365*.
- [34] S. Brodsky, *Phys. Rep.* **301**, 299 (1998).
- [35] S. D. Glazek, *Phys. Rev. D* **69**, 065002 (2004).
- [36] G. Altarelli and G. Parisi, *Nucl. Phys.* **B126**, 298 (1977).
- [37] K. G. Wilson, T. S. Walhout, A. Harindranath, W.-M. Zhang, R. J. Perry, and S. D. Glazek, *Phys. Rev. D* **49**, 6720 (1994).
- [38] S. D. Glazek (to be published).